International Journal of Bifurcation and Chaos, Vol. 31, No. 9 (2021) 2150131 (17 pages)

DOI: 10.1142/S0218127421501315

Fixed-Time Synergetic Control-Based Chaos Suppression for Eighth-Order IFOCIM Drive System

Ahmed Sadeq Hunaish* and Fadhil Rahma Tahir†
Electrical Engineering Department,
University of Basrah, Basrah, Iraq
**ahm782013@gmail.com*
†*fadhilrahma.creative@gmail.com*

Received ; Revised

This paper investigates chaos suppression in widely used indirect field oriented controlled induction machine (IFOCIM) drive system using fixed-time synergetic control method. The complex eighth-order IFOCIM drive system shows chaotic oscillations during a specific range of the integral gain of the PI speed controller. The conventional synergetic control method is improved by employing the fixed-time theory, the characteristics of the designed controller are chattering free and the convergence time is limited within a fixed-time upper bound depending on the controller parameters. The fixed-time synergetic control method is used to converge a selected macro variable to the origin within the fixed time upper bound. The controller can stabilize the chaotic system dynamics in a good way within a short time.

Keywords: Indirect field oriented controlled induction machine; choas suppression; fixed time theory; synergetic control.

1. Introduction

Induction machines (IM) as electrical to mechanical power conversion devices are used widely in industrial and domestics applications. Also, the indirect field oriented controlled induction machine (IFOCIM) is used widely in industrial applications due to its high torque response features. The nonlinear systems such as induction machines show very complex dynamics. The induction machine parameters are changed with time due to aging, heat rise during operation for long periods of time, saturation level, and environmental impact [Krishnan & Bharadwaj, 1991; Gao & Chau, 2003; Chua & Wang, 2011; Zhao *et al.*, 2016]. These changes in the parameters of the induction machine drive system may be lead to system variables bifurcation [Bazanella & Reginatto, 2000; Lu *et al.*, 2009; Salas *et al.*, 2008]. Also, the controller parameters variation of IFOCIM may be making the system dynamics bifurcate in cyclic or chaotic manner [Asakura *et al.*, 2000; Lu *et al.*, 2009; Gao & Chau, 2003]. Therefore, the elimination of chaos in the indirect field oriented controlled induction machine indicates interesting research in power conversion systems.

Many control techniques have been used in closed loop machine speed control to suppress the chaotic behavior. Few of these techniques are related to the induction machines. Therefore, beside IM, the survey will touch on permanent magnet

*Author for correspondence

synchronous machine (PMSM), brushless DC (BLDC) machine, and power systems which have similar dynamics behavior.

Asakura *et al.* [2000] used vector-control technique to control velocity of a reduced order IM with periodic speed reference, the controlled system dynamics had a chaotic oscillation due to identified error of the real rotor resistor value and the value in the controller, they employed three-layer neural network to control the chaos of the obtained third-order system. Ozer and Akin [2008] implemented a third-order oriented vector-controlled induction machine voltage mode observer, they used Pyragas control to suppress the chaotic state, the idea is to stabilize the unstable orbits that embedded in the chaotic system by using feedback of the states. Chen *et al.* [2012] used SMC to synchronize and eliminate the chaos in reduced order (fourth-order) field-oriented induction machine. Ranjbar and Kholerdi [2016] proposed a fuzzy controller to omit chaos in three-phase IM that is driven by constant voltage to frequency (V/f) inverter.

Harb [2004] suggested backstepping nonlinear control technique and sliding mode control (SMC) to eliminate chaos behavior in a permanent magnet synchronous machine (PMSM), the study stated that the backstepping nonlinear controller is much better than the SMC. Ren and Liu [2006] proposed nonlinear feedback control method to control the chaotic behavior in PMSM. Zribi *et al.* [2009] provided PMSM control method based on the instantaneous Lyapunov exponents (ILEs) algorithm to adjust the gain of the controller to make the positive (chaotic state) and zero instantaneous Lyapunov exponents negative (stable state). Huang *et al.* [2011] suggested a quasi-sliding mode control (QSMC) to suppress chaos for a PMSM, the QSMC forcing the system states to the quasisliding manifold by designing a continuous controller of the switching surface. Yu *et al.* [2012, 2015] employed neural networks to identify unknown and desired control signals and an adaptive tracking controller is constructed via backstepping for PMSM, the proposed adaptive neural controllers guarantee that the tracking error converges to a small neighborhood of the origin. Yu *et al.* [2016] introduced an adaptive fuzzy control technique with reduced order (fourth-order) observer method to eliminate the chaotic behavior in the dynamics of PMSM drive system. Borah and Roy [2017] used predictive control to control the chaos in permanent magnet synchronous generator (PMSG) where the simulation result is validated experimentally by implementing the electronic circuit. All the mentioned PMSM control techniques are used to control third-order systems. Rongyun *et al.* [2020] controlled the chaotic behavior in third-order PMSM by using synthetical SMC with inverse system decoupling, where they used SMC and super-twisting SMC for d-axes current and motor speed, respectively.

SMC, robust control and extended backstepping control were simulated numerically to control the chaos for third-order BLDC motor [Rajagopal *et al.*, 2017], the robust control was designed as SMC combined with field-oriented theory [Barambones *et al.*, 2012] while the backstepping control is desired to track a smooth periodic signal.

SMC with fixed-time control method was introduced to control sixth-order power system, numerical results show that the system chaos is stabilized in finite time [Ni *et al.*, 2017]. Wang *et al.* [2018] designed an adaptive feedback control system based on the finite time theory and the passivity-based approach for suppressing the chaos behavior in fourth-order power system. Zribi *et al.* [2018] provided a discrete SMC technique to bring order to the fourth-order chaotic power system, the two discrete SMC (DSMC) techniques exponential-reaching law and developed double power-reaching law were compared where the results show better reduced chattering response from the last method. Pole placement-based proportional integral SMC (PISMC) method was illustrated numerically to control chaotic oscillation in fourth-order power system, the simulation results stated that the chattering is reduced compared with conventional SMC method [Kumar & Singh, 2019]. Adaptive SMC method based on relay function was used to stabilize a second-order chaotic power system model, the adaptive method was employed to reduce the chattering effect that is caused by the conventional SMC method [Shang *et al.*, 2020]. Wang *et al.* [2020] designed the disturbance observer and SMC, which did not include the system equations, for second-order system and applied them to the seventh order power system. Two methods were used, linear state feedback control and dither control, to turn the chaotic state in sixth-order power system model into the periodic steady-state [Chang, 2020].

All the control strategies that were discussed have some advantages and disadvantages, these characteristics will be viewed alone here.

Neural Network (NN) can be developed by using different training algorithms, it can reveal complex nonlinear relations between dependent and independent variables, and it can be developed with less statistical training, while its drawbacks can be pointed as: it has unexpected behavior, there is not specific procedure to select the NN size, and needs more time for training [Tu, 1969]. The Pyragas method algorithm looks simple but it is sensitive to parameter choice [Fradkov & Evans, 2005]. SMC is a robust nonlinear control method with parameter uncertainty and simple implementation but the chattering phenomenon emerges [Huang *et al.*, 2020; Wang *et al.*, 2019]. Fuzzy control method is characterized by describing an inaccurate model, robust, with strong fault tolerance and some drawbacks such as the requirement of expert experience, difficult parameters tuning, decreasing the response speed with increase of accuracy, and hard realization [Huang *et al.*, 2020]. The backstepping nonlinear control method is a robust control technique with two drawbacks: the consumed time of the analytic calculation of control signal derivatives and the limitation to nonlinear systems that formed as a lower-triangular [Sonneveldt *et al.*, 2007]. Adaptive control methods are robust control methods and simple to use but they have some disadvantages as they undergo nonlinear-disturbances, are sensitive to noise, and require large memory [Yao *et al.*, 2015], sensitive to the adaptation values of the gains [Landau & Lozano, 1981], the adaptative rate is slow, and the transient response is poor [Cezayirli & Ciliz, 2008]. Predictive control is able to describe the inaccurate model and is robust but has slow response, complex structure, and hard realization [Huang *et al.*, 2020]. In PISMC, the chattering effect is reduced compared with conventional SMC method but not eliminated. The drawbacks of the disturbance observer and SMC method in [Wang *et al.*, 2020] are (1) the chattering effect due to SMC where its parameters must be adjusted to balance between low chattering and small steady-state error. (2) Also, to increase the observer accuracy by adjusting its parameters, the controller energy increases. The drawbacks of the state-feedback controller are: the constraints for the variables of the state and controller, decreasing the robustness with perturbations, and the need to find the coefficients of controller [Tarczewski & Grzesiak, 2016; Tahoumi *et al.*, 2018], while dither has two disadvantages include increase in the quantization of noise energy and dataacquisition times [Gray & Stockham, 1993; Chen *et al.*, 2020].

In all the reviewed control techniques besides the mentioned drawbacks, the steady state time response cannot be limited and cannot be expected, depending on initial conditions and system parameters. Also, the system contains chattering as noted in SMC and PISMC. Fixed-time synergetic control method can overcome these shortages when it reaches the steady state within fixed-time, independent of initial conditions, and it is chattering free. These properties make the fixed-time synergetic control (FTSC) method very suitable to suppress chaos in IFOCIM drive system.

A fixed-time synergetic control method has been used in this paper to suppress the chaotic phenomenon in complex eighth-order IFOCIM drive system, where the conventional synergetic control is improved by fixed-time theory. FTSC stability is also proved based on Lyapunov stability theory. In this paper, there are three main contributions to be mentioned as following: (1) chaos suppression in eighth-order IFOCIM drive system model is introduced and to the best of our knowledge, the model has not been controlled yet. (2) the synergistic control theory is employed to control the model. (3) The fixed-time theory is used to limit synergetic control time response within a fixed-time upper bound which depends only on the controller parameter regardless of the initial conditions

The remaining sections of this paper are divided into: The nonlinear model of the IFOCIM drive system is derived in Sec. 2, the model consists of eighth-order differential equations. Section 3 shows the dynamic behavior of IFOCIM due to control and motor parameters changes, the bifurcation diagram, Lyapunov exponents spectrum, basins of attractions, and phase portrait are used to show the bifurcation behavior of the system. Section 4 illustrates the proposed FTSC method and the FTSC is implemented to stabilize the eighth-order IFOCIM drive system with the proofs. In Sec. 5, FTSC is used to suppress the chaotic oscillation in IFOCIM drive system, the simulation results state that the system is stabilized within the proved time range without chattering. The conclusion is given in Sec. 6.

2. IFOCIM Drive System Modeling

The common closed loop control diagram of IFOCIM drive is shown in Fig. 1. The measured

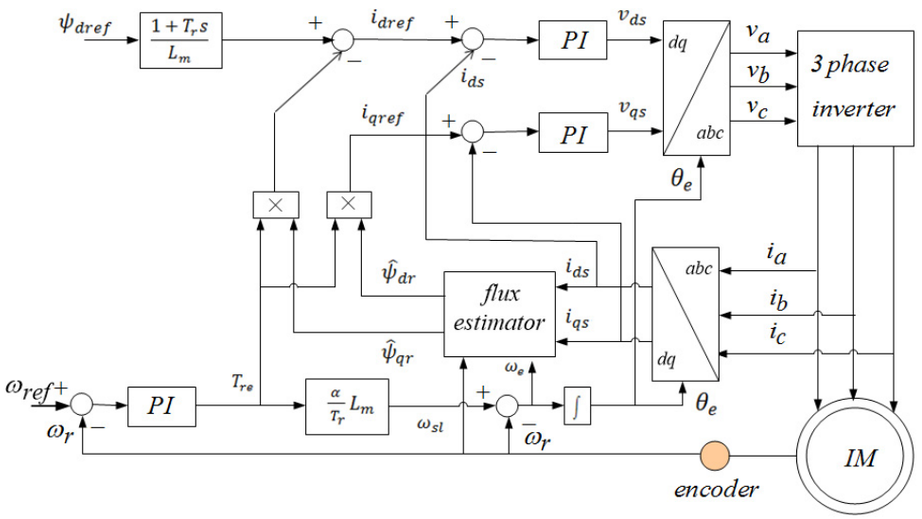

Fig. 1. IFOCIM drive system scheme.

speed and estimated flux signals are fed into the controller, and the stator current components (i_{ds} and i_{qs}) are produced from the flux and speed PI controllers. The inverter output is applied to IM, while the controller feedback signals are the stator currents of the induction motor. Also, the encoder (shaft encoder) is used to measure the shaft speed. Shaft encoder is a transducer that converts the angular speed of the shaft to analog or digital signal. The synchronous $d-q$ reference frame model of a squirrel-cage induction motor can be stated [Bose, 2001], to have the following full order IM dynamic system:

$$\frac{\mathrm{d}i_{ds}}{\mathrm{d}t} = -\gamma i_{ds} + \omega_e i_{qs} + \zeta\beta\psi_{dr} + \beta\omega_r\psi_{qr} + \frac{v_{ds}}{\sigma L_s}, \quad (1)$$

$$\frac{\mathrm{d}i_{qs}}{\mathrm{d}t} = -\omega_e i_{ds} - \gamma i_{qs} - \beta\omega_r\psi_{dr} + \zeta\beta\psi_{qr} + \frac{v_{qs}}{\sigma L_s}, \quad (2)$$

$$\frac{\mathrm{d}\psi_{dr}}{\mathrm{d}t} = \zeta L_m i_{ds} - \zeta\psi_{dr} + (\omega_e - \omega_r)\psi_{qr}, \quad (3)$$

$$\frac{\mathrm{d}\psi_{qr}}{\mathrm{d}t} = \zeta L_m i_{qs} - (\omega_e - \omega_r)\psi_{dr} - \zeta\psi_{qr}, \quad (4)$$

$$\frac{\mathrm{d}\omega_r}{\mathrm{d}t} = \frac{P}{2J}\left[\frac{3}{2}\frac{P}{2}\frac{L_m}{L_s}(\psi_{dr}i_{qs} - \psi_{qr}i_{ds}) - T_L - \frac{2}{P}B_m\omega_r\right], \quad (5)$$

where, v_{ds}, v_{qs}, ψ_{dr}, and ψ_{qr} are the stator voltage and the rotor fluxes in synchronous direct and quadrature axis reference frames to the stator, respectively; ω_e is the angular synchronous speed of the motor, $\sigma = 1 - \frac{L_m^2}{L_s L_r}$, $T_r = \frac{L_r}{R_r}$, $\gamma = \frac{R_s}{\sigma L_s} + \frac{1-\sigma}{\sigma T_r}$, $\beta = \frac{Lm}{\sigma L_s L_r}$, and $\zeta = \frac{1}{T_r}$. The motor parameters are listed in Table 1.

To compensate for the produced error between the estimated and real value of rotor resistance due to prolonged operation, the slip speed (ω_{sl}) in IFOCIM technique is described as follows

Table 1. System parameter definitions.

Parameter	Definition	Parameter	Definition
R_s	Stator resistor	P	Number of poles
L_s	Stator inductance	J	Rotor inertia
R_r	Rotor resistance	B_m	Viscous friction coefficient
L_r	Rotor inductance	T_r	Rotor time constant
L_m	Mutual inductance	T_l	Load torque
ω_r	Rotor speed	ω_{ref}	Speed reference

[Chua & Wang, 2011]:

$$\left.\begin{aligned}\omega_{sl} &= (\omega_e - \omega_r) = \frac{\alpha}{T_r} L_m T_{re} \\ T_{re} &= \left(K_{pw} + K_{iw}\int \mathrm{d}t\right)(\omega_{ref} - \omega_r)\end{aligned}\right\}. \quad (6)$$

The $d-q$ current components of the stator in the synchronous reference can be expressed as follows:

$$\left.\begin{aligned} i_{dref} &= \frac{\psi_{dref} + T_r \dot{\psi}_{dref}}{L_m} - \psi_{qr} T_{re} \\ i_{qref} &= \psi_{dr} T_{re}\end{aligned}\right\}, \quad (7)$$

where α is the gain of the compensator, ψ_{dref} is the rotor reference flux, $K_{p\omega}$ and $K_{i\omega}$ are the proportional and integral gains of the speed controller, respectively. From Fig. 1, Eqs. (1)–(7), and by defining the state variables $x_1 = i_{ds}$, $x_2 = i_{qs}$, $x_3 = \psi_{dr}$, $x_4 = \psi_{qr}$, $x_5 = \omega_r$, $x_6 = (K_{pw} + K_{iw}\int \mathrm{d}t)(\omega_{ref} - \omega_r)$, $x_7 = \int (i_{dref} - i_{ds})\mathrm{d}t$, and $x_8 = \int (i_{qref} - i_{qs})\mathrm{d}t$, the higher order model (HOM) of IFOCIM system can be expressed by the following equations:

$$\begin{aligned}\dot{x}_1 = &-\gamma x_1 + \left[x_5 + \frac{\alpha}{T_r} L_m x_6\right] x_2 + \frac{\beta}{T_r} x_3 \\ &+ \beta \frac{L_r}{L_m} Kpd \left[\frac{1}{L_m}\psi_{dref} + \frac{T_r}{L_m}\dot{\psi}_{dref}\right. \\ &\left. - x_4 x_6 - x_1\right] + \beta x_5 x_4 + \beta \frac{L_r}{L_m} K_{id} x_7, \quad (8)\end{aligned}$$

$$\begin{aligned}\dot{x}_2 = &-\left[x_5 + \frac{\alpha}{T_r} L_m x_6\right] x_1 - \gamma x_2 - \beta x_5 x_3 \\ &+ \frac{\beta}{T_r} x_4 + \beta \frac{L_r}{L_m} Kpq \left[x_3 x_6 - x_2\right] \\ &+ \beta \frac{L_r}{L_m} K_{iq} x_8, \quad (9)\end{aligned}$$

$$\dot{x}_3 = \frac{L_m}{T_r} x_1 - \frac{1}{T_r} x_3 + \frac{\alpha}{T_r} L_m x_4 x_6, \quad (10)$$

$$\dot{x}_4 = \frac{L_m}{T_r} x_2 - \frac{1}{T_r} x_4 - \frac{\alpha}{T_r} L_m x_3 x_6, \quad (11)$$

$$\dot{x}_5 = \frac{P}{2J}[K(x_2 x_3 - x_1 x_4) - T_L] - \frac{B_m}{J} x_5, \quad (12)$$

$$\begin{aligned}\dot{x}_6 = &-K_{pw}\left[\frac{P}{2J}[K(x_2 x_3 - x_1 x_4) - T_L] - \frac{B_m}{J} x_5\right] \\ &+ K_{iw}(\omega_{ref} - x_5), \quad (13)\end{aligned}$$

$$\dot{x}_7 = -x_1 - x_4 x_6 + \frac{1}{Lm}\psi_{dref} + \frac{T_r}{L_m}\dot{\psi}_{dref}, \quad (14)$$

$$\dot{x}_8 = -x_2 + x_3 x_6, \quad (15)$$

where $K = \frac{3}{2}\frac{P}{2}\frac{L_m}{L_r}$, K_{pd}, K_{id}, K_{pq}, and K_{iq} are the proportional and integral gains for the i_{ds}, i_{qs} controllers, respectively.

3. Dynamical Analysis

The IM parameters are listed in Table 2 [Gao & Chau, 2003] and the PI controller gains are chosen to be $K_{pd} = K_{pq} = 50$, $K_{id} = K_{iq} = 100$, $K_{p\omega} = 20$, $K_{i\omega} = 90$, $\psi_{dref} = 0.55\,\mathrm{Wb}$, and $\alpha = 1.3$. The speed reference and load torque are selected to be 50 rad/sec and 3 Nm, respectively.

3.1. *Equilibrium points*

Let the notations x_i^e, $i = 1, 2, \ldots, 8$ indicate the equilibrium point states. By considering $x_5^e = \omega_{ref}$ and solving (8) to (15), the vector values of the equilibrium point can be found as below:

$$X^e = \begin{bmatrix} x_1^e \\ x_2^e \\ x_3^e \\ x_4^e \\ x_5^e \\ x_6^e \\ x_7^e \\ x_8^e \end{bmatrix} = \begin{bmatrix} \dfrac{-m \pm \sqrt{m^2 - 4ln}}{2l} \\ \dfrac{B_m \omega_{ref} + \dfrac{P}{2} T_L}{\alpha \dfrac{P}{2} K \psi_{dref}} \\ L_m x_1^e (1-\alpha) + \alpha \psi_{dref} \\ L_m x_2^e (1-\alpha) \\ \omega_{ref} \\ \dfrac{x_2^e}{x_3^e} \\ \dfrac{L_m}{\beta L_r K_{id}}\left(a_1 x_1^e + a_2 \dfrac{(x_2^e)^2}{x_3^e} - a_3\right) \\ \dfrac{L_m}{\beta L_r K_{iq}}\left(\left(b_1 + b_2 \dfrac{x_2^e}{x_3^e}\right) x_1^e + b_3\right) \end{bmatrix}, \quad (16)$$

Table 2. IM parameters for simulation.

Parameter	Value	Parameter	Value
P	4	L_r (H)	0.2235
R_s (Ω)	0.76	L_m (H)	0.2176
L_s (H)	0.2248	J (kgm^2)	0.0111
R_r (Ω)	0.675	B_m (Nm/rad/s)	7.355×10^{-4}

where

$$l = (1-\alpha)L_m^2,$$

$$m = (2\alpha - 1)L_m\psi_{dref},$$

$$n = \frac{l\left(B_m\omega_{ref} + \frac{P}{2}T_L\right)^2}{\left(\alpha\frac{P}{2}K\psi_{dref}\right)^2} - \alpha\psi_{dref}^2,$$

$$a_1 = \gamma - \beta\frac{L_m}{T_r}(1-\alpha) + \frac{\beta L_r}{L_m}K_{pd},$$

$$a_2 = \beta L_r(1-\alpha)K_{pd} - \alpha\frac{L_m}{T_r},$$

$$a_3 = (\beta L_m(1-\alpha)+1)\omega_{ref}\frac{B_m\omega_{ref} + \frac{P}{2}T_L}{\alpha\frac{P}{2}K\psi_{dref}} + \left(\frac{\alpha\beta}{T_r} + \frac{\beta L_r K_{pd}}{L_m^2}\right)\psi_{dref},$$

$$b_1 = \omega_{ref} + \beta\omega_{ref}L_m(1-\alpha),$$

$$b_2 = \frac{\alpha L_m}{T_r} \quad \text{and}$$

$$b_3 = \left(\gamma - \frac{\beta L_m}{T_r}(1-\alpha)\right)\frac{B_m\omega_{ref} + \frac{P}{2}T_L}{\alpha\frac{P}{2}K\psi_{dref}} + \alpha\beta\omega_{ref}\psi_{dref}.$$

From (16), X^e is not unique for $\alpha \neq 1$, otherwise X^e has a unique solution. The real solution of X^e is obtained when:

$$\frac{2L_m\left(B_m\omega_{ref} + \frac{P}{2}T_L\right)}{2L_m\left(B_m\omega_{ref} + \frac{P}{2}T_L\right) + \frac{P}{2}K\psi_{dref}^2} \leq \alpha \leq \frac{2L_m\left(B_m\omega_{ref} + \frac{P}{2}T_L\right)}{2L_m\left(B_m\omega_{ref} + \frac{P}{2}T_L\right) - \frac{P}{2}K\psi_{dref}^2}. \tag{17}$$

According to (17), the real solution is obtained in the range of $0.61 \leq \alpha \leq 3.04$. Outside of this range of α, the system does not have real equilibrium points.

3.2. *Stability of equilibrium points*

The PI controller gains are chosen to be $K_{pd} = K_{pq} = 50$, $K_{id} = K_{iq} = 100$, $K_{p\omega} = 20$, and $0 \leq K_{i\omega} \leq 120$, while $\psi_{dref} = 0.55\,\text{Wb}$, and $\alpha = 1.3$. According to (16) the system has two different equilibrium points:

$$X^{e1} = (2.783, 1.446, 0.533, -0.094, 50, 2.71, 0.12, -0.531)^T$$

$$X^{e2} = (10.697, 1.446, 0.017, -0.094, 50, 86.561, 0.344, -0.13)^T$$

Based on the linearization theorem, the differential system can be described in matrix form close to the equilibrium point as follows:

$$\dot{x} = J(x)x, \tag{18}$$

where $J(x)$ is the Jacobian matrix of the system and $x = (x_1, x_2, x_3, x_4, x_5, x_6, x_7, x_8)^T$ is the vector of the system variables. The Jacobian matrix of the linearized model can be given as:

$$J(x) = \begin{bmatrix} J_{6\times6} & J_{6\times2} \\ J_{2\times6} & 0_{2\times2} \end{bmatrix}, \tag{19}$$

where,

$$J_{6\times6}=\begin{bmatrix} -\gamma-c_1K_{pd} & x_5^e+c_2x_6^e & \dfrac{\beta}{T_r} & \beta x_5^e-c_1K_{pd}x_6^e & -x_2^e-\beta x_4^e & c_2x_2^e-c_1K_{pd}x_4^e \\ -x_5^e-c_2x_6^e & -\gamma-c_1K_{pq} & c_1K_{pq}x_6^e-\beta x_5^e & \dfrac{\beta}{T_r} & x_1^e+\beta x_3^e & -c_2x_1^e+c_1K_{pq}x_3^e \\ \dfrac{c_2}{\alpha} & 0 & \dfrac{-1}{T_r} & c_2x_6^e & 0 & c_2x_4^e \\ 0 & \dfrac{c_2}{\alpha} & -c_2x_6^e & \dfrac{-1}{T_r} & 0 & -c_2x_3^e \\ c_4x_4^e & -c_4x_3^e & -c_4x_2^e & c_4x_1^e & -c_3 & 0 \\ c_4K_{pw}x_4^e & -c_4K_{pw}x_3^e & -c_4K_{pw}x_2^e & c_4K_{pw}x_1^e & K_{iw}-c_3K_{pw} & 0 \end{bmatrix},$$

$$J_{6\times2}=\begin{bmatrix} c_1K_{id} & 0 & 0 & 0 & 0 & 0 \\ 0 & c_1K_{iq} & 0 & 0 & 0 & 0 \end{bmatrix}^T, \quad J_{2\times6}=\begin{bmatrix} -1 & 0 & 0 & -x_6^e & 0 & -x_4^e \\ 0 & -1 & x_6^e & 0 & 0 & x_3^e \end{bmatrix},$$

$$c_1=\beta\frac{L_r}{L_m}, \quad c_2=\alpha\frac{L_m}{T_r}, \quad c_3=\frac{B_m}{J} \quad \text{and} \quad c_4=\frac{1.5L_mP^2}{4JL_r}.$$

The eigenvalues of the Jacobian matrix described in (19) are checked numerically. The equilibrium point X^{e1} is stable while X^{e2} is unstable for $K_{i\omega} > 106.4$. For $K_{i\omega} = 106.4$, the eigenvalues are listed in Table 3.

3.3. *Bifurcation diagrams and Lyapunov exponents*

The IFOCIM model specified by (8)–(15) has been numerically investigated for different values of the controller parameters. The bifurcation diagram and corresponding Lyapunov exponents spectrum as a function of parameter α are shown in Fig. 2. The parameters are $K_{pd} = K_{pq} = 50$, $K_{id} = K_{iq} = 100$, $K_{p\omega} = 20$, $K_{i\omega} = 90$, and $\psi_{dref} = 0.55$ Wb. From Fig. 2, one can note that, for a certain value of controller gains with varying α, the system bifurcates into period-1, period-2, period-3 and chaotic attractor. When α is varied from 0.3 to 5, Figs. 2(a) and 2(b) depict that the dominant cases are period-1, period-2, period-3, and period-4 in the ranges of α from 0.3 to 0.725 and from 1.327 to 5 and the fixed point is seen in the range from 0.726 to 1.284, while chaos is noted during the tiny range from 1.285 to 1.326 only. The results show that chaos occurs in very small range of α, while it is noted that the results in the previous studies [Bazanella & Reginatto, 2000; Lu *et al.*, 2009; Jain *et al.*, 2018] showed that in the general behavior of the system, saddle-node bifurcation (SNB), Hopf bifurcation (HB), Bogdanov–Takens (BTB), and zero Hopf bifurcation (ZHB) occur.

As shown in Fig. 2, the value of α which leads to chaos is varied in a small range around 1.3 for $K_{i\omega} = 90$. Besides, in practical applications, the

Table 3. The eigenvalues of the linearized system for $K_{pd} = K_{pq} = 50$, $K_{id} = K_{iq} = 100$, $K_{p\omega} = 20$, $K_{i\omega} = 106.4$, $\psi_{dref} = 0.55$ Wb, $\alpha = 1.3$, $T_l = 3$ Nm and $\omega_{ref} = 50$ rad/sec.

Eigenvalues	X^{e1}	X^{e2}
λ_1	-7832.1	$-7785.7+175.27i$
λ_2	$-3913.8+2914i$	$-7785.7-175.27i$
λ_3	$-3913.8-2914i$	-71.9
λ_4	$-0.487+0.064i$	-38.644
λ_5	$-0.487-0.064i$	$+14.707$
λ_6	-2.81	-5.125
λ_7	-4.175	$-0.468+0.047i$
λ_8	-5.322	$-0.468-0.047i$

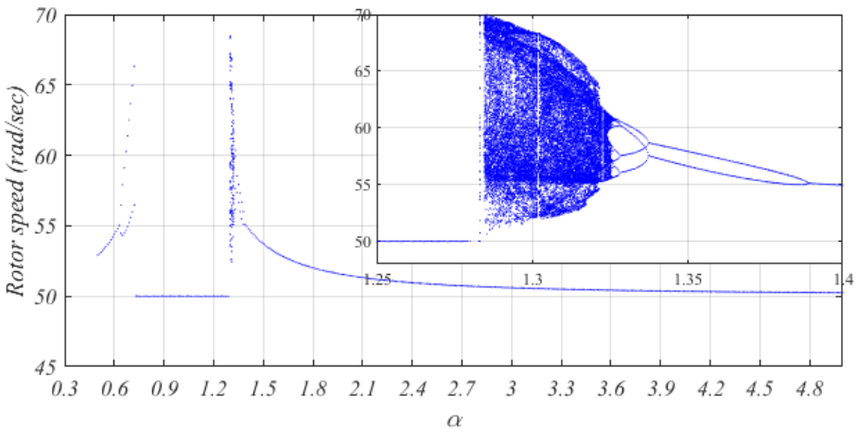

(a)

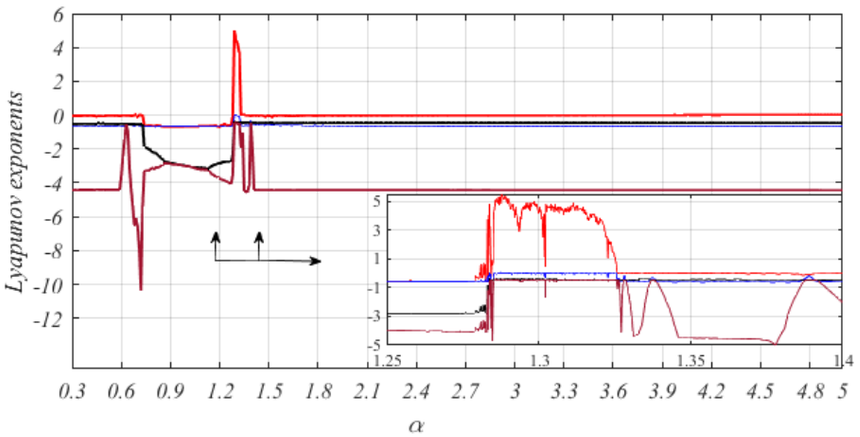

(b)

Fig. 2. Speed bifurcation diagram and Lyapunov exponents due to α change at $K_{pd} = K_{pq} = 50$, $K_{id} = K_{iq} = 100$, $K_{p\omega} = 20$, and $K_{i\omega} = 90$ (a) bifurcation diagram and (b) the first four corresponding Lyapunov exponents.

upper limit value of α is about 1.5 [Krishnan & Doran, 1987]. Therefore, $\alpha = 1.3$ is selected to investigate the system dynamics due to the changes of the controller gain(s).

The system dynamics are verified numerically to investigate the bifurcation behavior as $K_{i\omega}$ changes for a certain value of $\alpha(= 1.3)$ as illustrated in Fig. 3(a). It is noted that for $K_{i\omega} = 0$, a stable periodic solution occurs with period-2; period-doubling bifurcation route to chaos appears for $K_{i\omega} \geq 0.1$. Period-4 occurs for $K_{i\omega}$ from 0.1 to 23, period-8 for $K_{i\omega}$ from 23.1 to 28.3, and period-16 for $K_{i\omega}$ from 28.4 to 29.7. The system exhibits chaos for $K_{i\omega}$ from 29.8 to 106.3. While period-5 and period-10 are also noted at windows for $K_{i\omega}$ from 75.6 to 76.7 and $K_{i\omega}$ from 76.8 to 77.7, respectively. Period-10 range has been enlarged as in Fig. 3(a). Also, there are windows for fixed point spread between the chaos region for $K_{i\omega}$ from 104.3 to 104.6 and $K_{i\omega}$ from 104.9 to 105. For $K_{i\omega} \geq 106.4$, the system tracks speed command perfectly which is noted as the fixed point. The first four Lyapunov exponents are illustrated in Fig. 3(b) that validate the system behavior in Fig. 3(a). The chaotic attractors are demonstrated in Fig. 4. The three-dimensional (3D) phase portrait projected (i_{ds}, i_{qs}, ω_r) has been plotted for different values of K_{iw}: $K_{iw} = 50$ in Fig. 4(a) and $K_{iw} = 90$ in Fig. 4(b).

3.4. *Basins of attractions and multistability*

In this subsection, the basins of attractions and multistability will be discussed. As in other

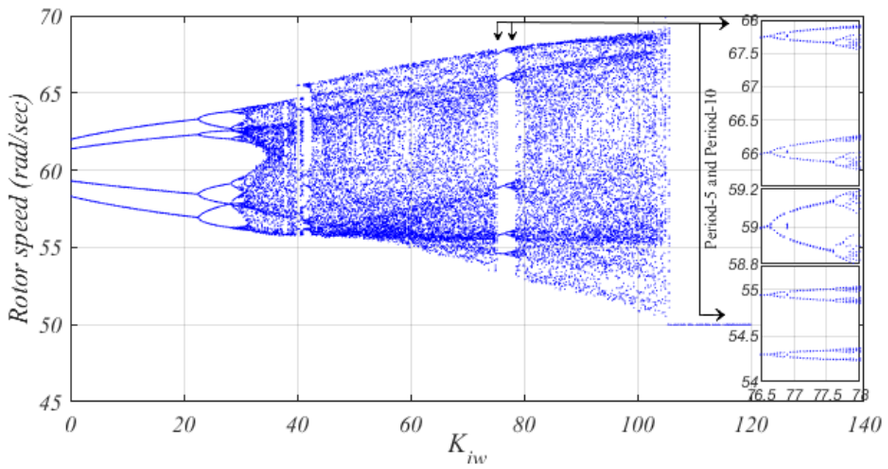

(a)

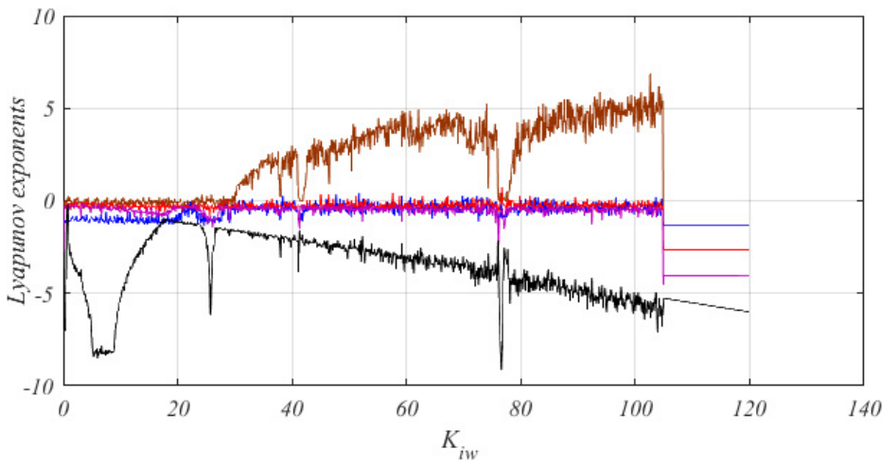

(b)

Fig. 3. IFOCIM drive system with $K_{pd} = K_{pq} = 50$, $K_{id} = K_{iq} = 100$, $K_{p\omega} = 20$, $\psi_{dref} = 0.55$ Wb, $\alpha = 1.3$, $\omega_{ref} = 50$ and $T_L = 3$ Nm (a) bifurcation diagram and (b) the corresponding spectrum of the first four Lyapunov exponents L_1, L_2, L_3, and L_4 illustrate various behaviors of system with variation of $K_{i\omega}$ upwards in the range $0 \leq K_{i\omega} \leq 120$.

nonlinear systems, the multistability and coexistence could be present. The nonlinear systems are sensitive to the change in its parameters and the initial conditions of the state variables. The numerical simulation has been used to investigate the different dynamic attractors for a certain values of the parameters. In Fig. 5, the system shows three different attractors: fixed point (blue), periodic (red) and chaotic (yellow). Figures 5(a)–5(c) represent different attractors with respect to the change in initial values of x_3 and x_4 with $K_{iw} = 20, 90$, and 106, respectively. The other variables have constant initial values $x_1(0) = 0$, $x_2(0) = 0$, $x_5(0) = 0$, $x_6(0) = 0$, $x_7(0) = 0$, and $x_8(0) = 0$. Figure 5(a) involves two different attractors, that are fixed point and periodic attractors each alone and as periodic attractors spread inside the area of the fixed point attractor. In Fig. 5(b), two attractors are present — periodic and chaotic. The chaotic attractor occupies a small region (yellow) which is collared by a large fixed point attractor area (blue). Also, Fig. 5(c) demonstrates two different attractors (chaotic and fixed point) for $K_{iw} = 106$ and initial states $(0, 0, x_3, x_4, 0, 0, 0, 0)$ where x_3 and x_4 are varied. While in Figs. 5(d)–5(f), the initial values of x_1, x_2, x_3, x_4, x_5, and x_8 have been adjusted to be 0, 0, 0, 0, 0, and 0, respectively, and the values of $x_6(0), x_7(0)$ are changed. Figure 5(d) illustrates

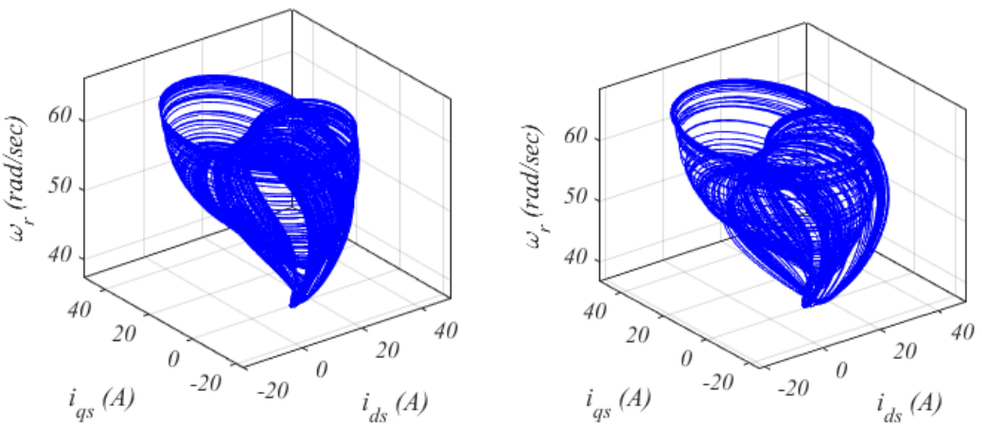

(a) (b)

Fig. 4. 3D Phase portrait projected $(i_{ds}, i_{qs}, \omega_r)$ with system parameters $K_{pd} = K_{pq} = 50$, $K_{id} = K_{iq} = 100$, $K_{p\omega} = 20$, $\psi_{dref} = 0.55\,\text{Wb}$, $\alpha = 1.3$; $T_L = 3\,\text{Nm}$ and $\omega_{ref} = 50\,\text{rad/sec}$: (a) $K_{i\omega} = 50$ and (b) $K_{i\omega} = 90$.

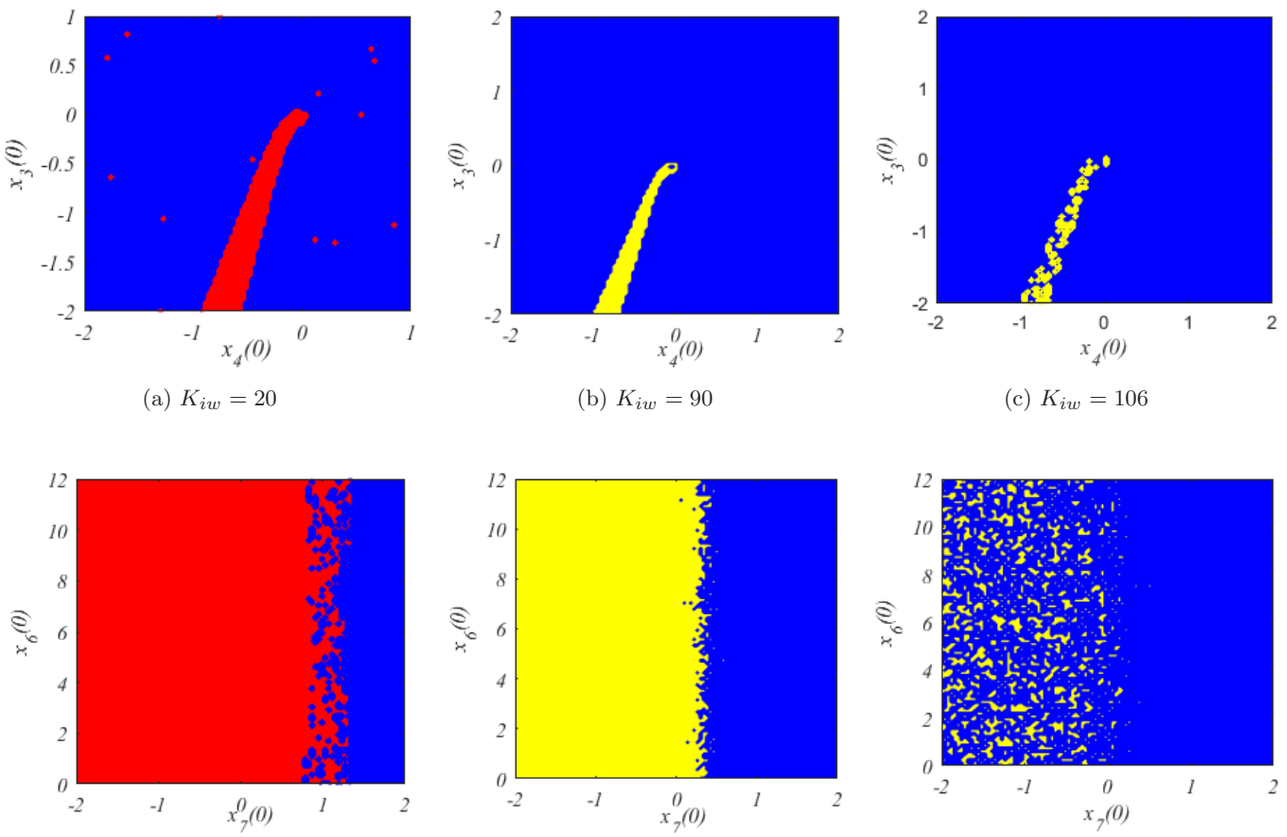

(a) $K_{iw} = 20$ (b) $K_{iw} = 90$ (c) $K_{iw} = 106$

(d) $K_{iw} = 20$ (e) $K_{iw} = 90$ (f) $K_{iw} = 106$

Fig. 5. Basins of attractions with system parameters as in Fig. 3 and $K_{i\omega}$ as mentioned in the subfigure lables, where in (a)–(c) x_3 and x_4 are varied with $x_1(0) = 0$, $x_2(0) = 0$, $x_5(0) = 0$, $x_6(0) = 0$, $x_7(0) = 0$, and $x_8(0) = 0$ and (d)–(f) x_6 and x_7 are varied with $x_1(0) = 0$, $x_2(0) = 0$, $x_3(0) = 0$, $x_4(0) = 0$, $x_5(0) = 0$, and $x_8(0) = 0$, fixed point (blue), periodic (red) and chaotic (yellow).

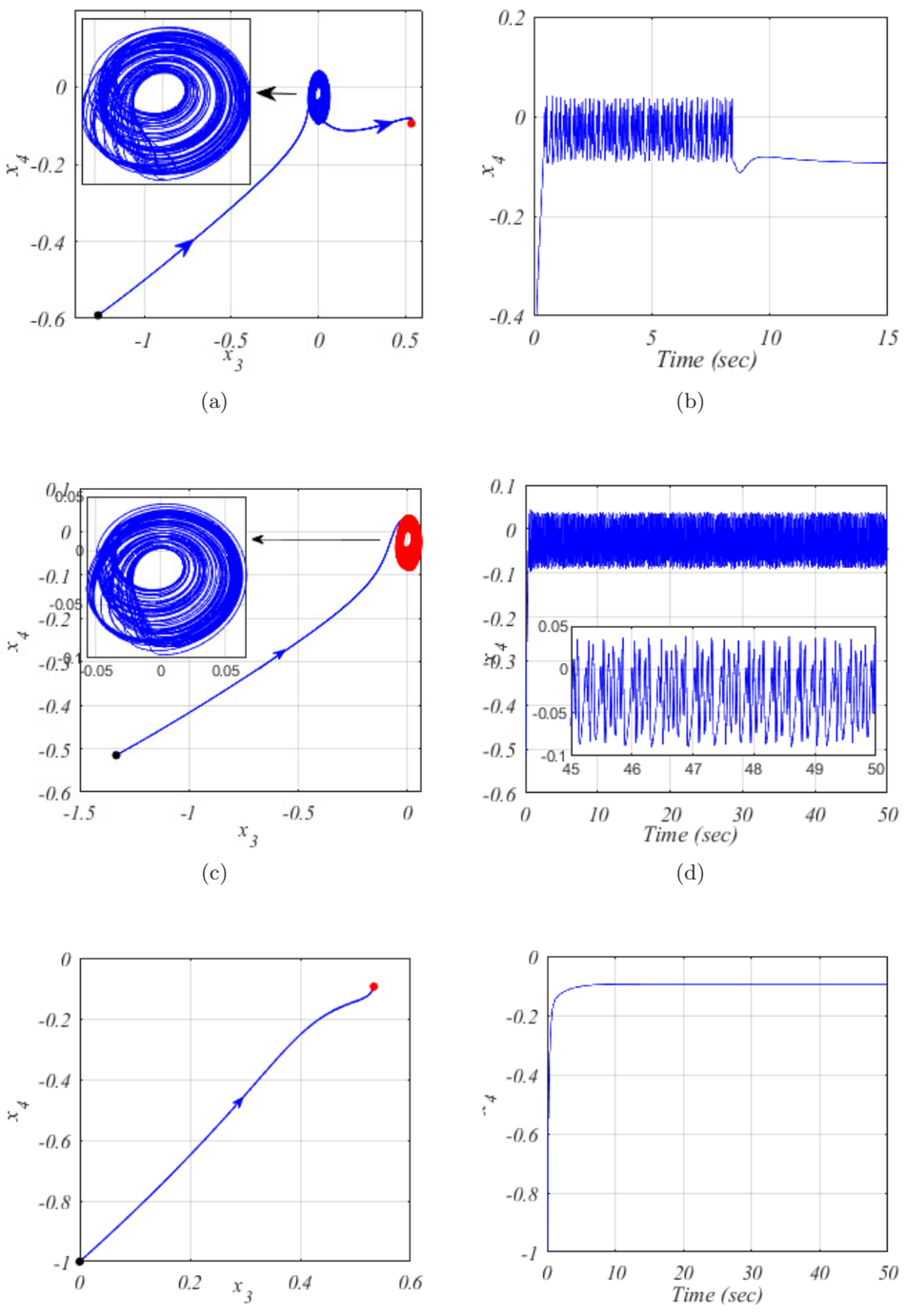

Fig. 6. Phase portrait and time series with system parameters $K_{pd} = K_{pq} = 50$, $K_{id} = K_{iq} = 100$, $K_{p\omega} = 20$, $\psi_{dref} = 0.55\,\text{Wb}$, $\alpha = 1.3$, $\omega_{ref} = 50$ and $T_L = 3\,\text{Nm}$: (a) phase portrait projection (x_3, x_4) shows transient chaotic behavior followed by steady-state behavior for $K_{i\omega} = 110$ and the initial value $(x_1(0), x_2(0), x_3(0), x_4(0), x_5(0), x_6(0), x_7(0), x_8(0)) = (0, 0, -1.265, -0.5918, 0, 0, 0, 0)$, (b) the corresponding time series of x_4, (c) phase portrait projection (x_3, x_4) for same parameter value with $K_{i\omega} = 90$ and $(x_1(0), x_2(0), x_3(0), x_4(0), x_5(0), x_6(0), x_7(0), x_8(0)) = (0, 0, -1.333, -0.5152, 0, 0, 0, 0)$, (d) the corresponding time series of x_4, (e) phase portrait projection (x_3, x_4) for same parameter value with $K_{i\omega} = 90$ and $(x_1(0), x_2(0), x_3(0), x_4(0), x_5(0), x_6(0), x_7(0), x_8(0)) = (0, 0, 0, -1, 0, 0, 0, 0)$ and (f) the corresponding time series of x_4.

the coexistence of two attractors, fixed point (blue) and periodic (red), when varying the initial values of x_6 and x_7 and keeping the others as mentioned earlier. Figure 5(e) displays fixed point and chaotic attractors due to the changes in the initial values of x_6 and x_7 for $K_{iw} = 90$. Also, Fig. 5(f) has a fixed point and chaotic attractors but for $K_{iw} = 106$. The chaotic attractors are represented in yellow as very small areas inside the blue fixed point attractor farm. These different attractors which are shown in Fig. 5 imply the sensitivity of the IFOCIM system to the variation in the initial values of IFOCIM system variables.

From Figs. 6(a) and 6(b), the system exhibits a transient chaotic behavior followed by fixed point steady-state behavior with system parameters as in Fig. 3 and $K_{i\omega} = 110$ while the initial value $(x_1(0), x_2(0), x_3(0), x_4(0), x_5(0), x_6(0), x_7(0), x_8(0)) = (0, 0, -1.265, -0.5918, 0, 0, 0, 0)$. For the same parameters above and $K_{i\omega} = 90$, the system has chaotic behavior as in Figs. 6(c) and 6(d) for $(x_1(0), x_2(0), x_3(0), x_4(0), x_5(0), x_6(0), x_7(0), x_8(0)) = (0, 0, -1.333, -0.5152, 0, 0, 0, 0)$ and it has fixed point behavior as in Figs. 6(e) and 6(f) for $(x_1(0), x_2(0), x_3(0), x_4(0), x_5(0), x_6(0), x_7(0), x_8(0)) = (0, 0, 0, -1, 0, 0, 0, 0)$. It is clear from Figs. 6(c)–6(f) the system has two different attractors for the same parameters when the initial values have been changed. From Figs. 3, 5, and 6, one can conclude that the IFOCIM model has multistability.

4. Controller Design

The fixed-time synergetic control has been used to control the complicated nonlinear system dynamics, FTSC idea is to design a macro variable ψ which introduces the control input $u(t)$ to drive the system dynamics to follow the command signal in a fixed-time upper bound.

4.1. *Fixed time theory*

Definition 4.1 [Ni *et al.*, 2017; Wang *et al.*, 2019]. Consider a nonlinear system described by:

$$\dot{x} = f(x), \quad x(0) = x_0 \tag{20}$$

where $x \in R$ and $f(x) \in R$.

Assume an equilibrium point of system (20) is the origin, then it is said to be a fixed-time stable equilibrium point provided that it is stable with bounded convergence time $T(x_0)$, that is $\exists T_{\max} > 0$, such that $\lim_{x_0 \to \infty}[T(x_0)] \leq T_{\max}$.

Lemma 1 [Ni *et al.*, 2017; Wang *et al.*, 2019; Huang *et al.*, 2020]. *Consider the system below*:

$$\dot{y} = -\alpha y^{\frac{m}{n}} - \beta y^{\frac{q}{p}}, \quad y(0) = y_0, \tag{21}$$

where α *and* β *are both* > 0 *and* m, n, q, p *are all positive odd integers, satisfying* $m > n$, $0 < q/p < 1$. *The system (21) is stabilizing to the origin in convergence time* $T(y_0)$, *then* y *will converge to the origin within a fixed time upper bound* $T_{\max}(y)$, *and by a constant* $T_{\max}(y)$, *that is* $\lim_{y_0 \to \infty}[T(y_0)] \leq T_{\max}(y)$, *and*

$$T_{\max}(y) = \frac{n}{\alpha(m-n)} + \frac{p}{\beta(p-q)}. \tag{22}$$

Lemma 2 [Wang *et al.*, 2019; Huang *et al.*, 2020]. *Consider a continuous positive definite function* V, *and assume it is satisfying the differential equation*:

$$\dot{V} = -\alpha_1 V^{\gamma_1} - \beta_1 V^{\gamma_2}, \quad V(0) = V_0, \tag{23}$$

where α_1 *and* β_1 *are positive real numbers,* γ_1 *and* γ_2 *are all positive real numbers, satisfying* $\gamma_1 > 1$, $0 < \gamma_2 < 1$.

The required time to converge the system (23) to the origin is set to be $T(V_0)$, *then* V *will converge to the origin within a fixed-time upper bound* $T_{\max}(V)$, *and by a constant* $T_{\max}(y)$, *that is* $\lim_{V_0 \to \infty}[T(V_0)] \leq T_{\max}(V)$, *and*

$$T_{\max}(V) = \frac{1}{\alpha_1(\gamma_1 - 1)} + \frac{1}{\beta_1(1 - \gamma_2)}. \tag{24}$$

4.2. *Design of fixed-time synergetic control for IFOCIM drive system*

Consider the following nonlinear system:

$$\left.\begin{aligned} \dot{x}_i &= x_{i+1}, \quad i = 1, 2, 3, \ldots, n-1 \\ \dot{x}_n &= f_n(x) + g(x)u \end{aligned}\right\}, \tag{25}$$

where $x = (x_1, x_2, \ldots, x_n)^T \in R$ is the state vector of the system, $f_n(x) \in R$ represents a nonlinear function that describes the dynamics of the system, $g_n(x) \neq 0$ is the control gain, and $u \in R$ stands for control input.

The control input u is designed practically, based on synergetic control theory (SCT) which includes the movement of the system dynamics to

invariant manifold from any initial vector, then the dynamics are pulled to the origin of the system (25). In order to move system dynamics (25) to the origin, a macro variable ψ must be defined to satisfy:

$$T\dot{\psi} + \phi(\psi) = 0, \tag{26}$$

where T is selected to be the design parameter that determines the convergence rate of macro variable ψ to the invariant manifold $\psi(0)$ and $\phi(\psi)$ is a differentiable function of ψ that must satisfy:

(1) invertible;
(2) $\phi(0) = 0$;
(3) $\phi(\psi)\psi > 0, \forall\, \psi \neq 0$.

Lemma 3 [Wang *et al.*, 2019]. *If the function $\phi(\psi)$ is defined as (27), then $\phi(\psi)$ satisfies the conditions*:

$$\phi(\psi) = \psi^{\frac{p_1}{q_1}} + \psi^{\frac{q_1}{p_1}}, \tag{27}$$

where q_1 and p_1 are odd numbers, and satisfy $0 < q_1/p_1 < 1$.

Then (26) of the macro variable can be rewritten by using (27) as follows:

$$T\dot{\psi} + \psi^{\frac{p_1}{q_1}} + \psi^{\frac{q_1}{p_1}} = 0. \tag{28}$$

From Lemma 1 and (28), the macro variable will reach the invariant manifold $\psi = 0$ in a fixed-time and settles down on the manifold forever. The convergence time is denoted by $T(\psi_0)$, then $\lim_{\psi_0 \to \infty}[T(\psi_0)] \leq T_{\max}(\psi)$ and

$$T_{\max}(\psi) = T\left(\frac{p_1 + q_1}{p_1 - q_1}\right). \tag{29}$$

It is seen from (29), the manifold reaching time is determined by the parameters p_1, q_1, and T. Therefore, these parameters should be selected carefully to ensure that the macro variable gets the invariant manifold in shortest time as possible.

The control objective is to retrieve the state variables of IFOCIM drive system described by (8)–(15) from the chaotic behavior to stable equilibrium state. From Fig. 3 in Sec. 3.3, the changes in integral gain $K_{i\omega}$ of the PI speed loop which is described by (13) lead the system to chaotic oscillations, therefore, the control input $u(t)$ will be added to the speed loop controller section which can stabilize the chaotic dynamics. The controlled system can be described as:

$$\dot{x}(t) = f(x,t) + g(x)u, \tag{30}$$

where

$$f(x,t) = \begin{bmatrix}
-\gamma x_1 + \left[x_5 + \dfrac{\alpha}{T_r} L_m x_6\right] x_2 + \dfrac{\beta}{T_r} x_3 + \beta \dfrac{L_r}{L_m} Kpd\left[\dfrac{1}{L_m}\psi_{dref} + \dfrac{T_r}{L_m}\dot{\psi}_{dref} - x_4 x_6 - x_1\right] \\
\quad + \beta x_5 x_4 + \beta \dfrac{L_r}{L_m} K_{id} x_7 \\
-\left[x_5 + \dfrac{\alpha}{T_r} L_m x_6\right] x_1 - \gamma x_2 - \beta x_5 x_3 + \dfrac{\beta}{T_r} x_4 + \beta \dfrac{L_r}{L_m} Kpq[x_3 x_6 - x_2] + \beta \dfrac{L_r}{L_m} K_{iq} x_8 \\
\dfrac{L_m}{T_r} x_1 - \dfrac{1}{T_r} x_3 + \dfrac{\alpha}{T_r} L_m x_4 x_6 \\
\dfrac{L_m}{T_r} x_2 - \dfrac{1}{T_r} x_4 - \dfrac{\alpha}{T_r} L_m x_3 x_6 \\
\dfrac{P}{2J}[K(x_2 x_3 - x_1 x_4) - T_L] - \dfrac{B_m}{J} x_5 \\
-K_{pw}\left[\dfrac{P}{2J}[K(x_2 x_3 - x_1 x_4) - T_L] - \dfrac{B_m}{J} x_5\right] + K_{iw}(\omega_{ref} - x_5) \\
-x_1 - x_4 x_6 + \dfrac{1}{Lm}\psi_{dref} + \dfrac{T_r}{L_m}\dot{\psi}_{dref} \\
-x_2 + x_3 x_6
\end{bmatrix}$$

and

$$g(x) = [0, 0, 0, 0, 0, m_5, 0, 0]^T.$$

Let $y_1 = \omega_r - \omega_{ref}$, then the system dynamics can be written as follows:

$$\left.\begin{aligned} \dot{y}_1(t) &= y_2 \\ \dot{y}_2(t) &= f_9(x) + m_5 u(t) \end{aligned}\right\}, \tag{31}$$

where

$$\left.\begin{aligned} f_9 &= m_1 f_1 + m_2 f_2 + m_3 f_3 + m_4 f_4 + m_5 f_5 \\ m_1 &= c_4 x_4 \\ m_2 &= -c_4 x_3 \\ m_3 &= -c_4 x_2 \\ m_4 &= c_4 x_1 \\ m_5 &= -20 c_3 \end{aligned}\right\}.$$

The controller design for the system (31) requires a definition of an evident form for the macro variable ψ. There are many styles for selecting the macro variable ψ that can force the state variable of the system (31) converge asymptotically to the origin when the macro variable attains the invariant manifold $\psi = 0$. However, the simplest method used to select ψ is the linear combination of the system (31) state variables y_1 and y_2 as below:

$$\psi = k y_1 + y_2. \tag{32}$$

When the parameter k is selected to be positive, the state variables y_1 and y_2 of the system (31) converge asymptotically to the origin. The control input $u(t)$ can be obtained by combining (28) and (32) to get the control input as follows:

$$u(t) = -\frac{1}{m_5}\left(f_9 + k y_2 + \frac{1}{T}(\psi^{q_1/p_1} + \psi^{p_1/q_1})\right). \tag{33}$$

Theorem 1. *The given macro variable (32) reaches the invariant manifold $\psi = 0$ within a fixed-time if the control input of the system (31) is designed as in (33).*

Proof. Let a Lyapunov candidate function be defined as:

$$V = \frac{\psi^2}{2}. \tag{34}$$

Then the time derivative of (34) is:

$$\begin{aligned} \dot{V} &= -\frac{1}{T}(\psi^{(q_1/p_1+1)} + \psi^{(p_1/q_1+1)}) \\ &= -\frac{1}{T}((2V)^{\frac{q_1+p_1}{2p_1}} + (2V)^{\frac{q_1+p_1}{2q_1}}) \end{aligned} \tag{35}$$

Let $W = 2V$, then (35) becomes:

$$\begin{aligned} \dot{W} &= -\frac{1}{T}(W^{\frac{q_1+p_1}{2p_1}} + W^{\frac{q_1+p_1}{2q_1}}) \\ &= -\frac{1}{T}(W^{\zeta_1} + W^{\zeta_2}), \end{aligned} \tag{36}$$

where $\zeta_1 = \frac{q_1+p_1}{2p_1}$ and $\zeta_2 = \frac{q_1+p_1}{2q_1}$

According to Lemma 2, and since $\zeta_1 > 1$ and $0 < \zeta_2 < 1$ in (36), then the functions W and V converge to zero in a fixed-time, which means the selected macro variable ψ enters the invariant manifold $\psi = 0$ in a fixed-time too.

The proof is completed. ■

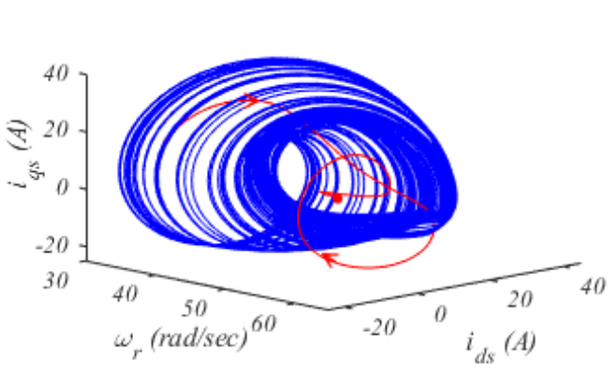

(a)

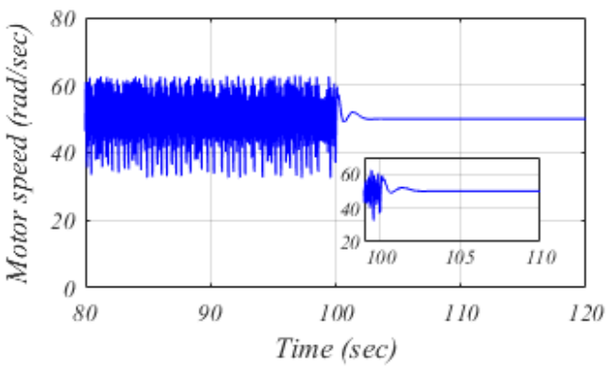

(b)

Fig. 7. System response when the control acts at $t = 100$ sec for system parameters as in Fig. 4(b) and the controller parameters are $k = 10$, $T = 1.21$, $p_1 = 9$, and $q_1 = 7$, (a) the phase portrait projection $(\omega_r, i_{ds}, i_{qs})$, (b) the time responses for motor speed, (c) d-component of stator current and (d) q-component of stator current.

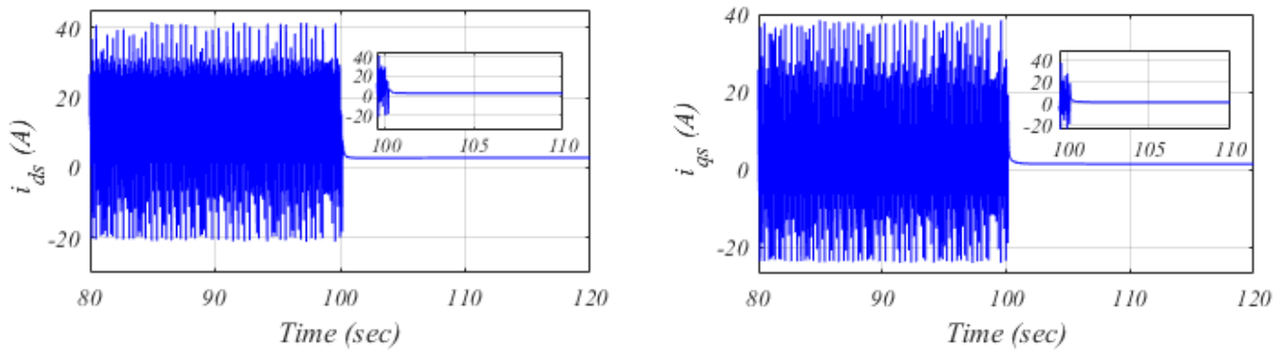

(c) (d)

Fig. 7. (*Continued*)

5. Simulation Results

The system has been simulated under control action to show the controller effectiveness. The system parameters are $K_{pd} = K_{pq} = 50$, $K_{id} = K_{iq} = 100$, $K_{p\omega} = 20$, $K_{i\omega} = 90$, $\psi_{dref} = 0.55$ Wb, and $\alpha = 1.3$, while the controller parameters have been selected to be $k = 10$, $T = 1.21$, $p_1 = 9$, and $q_1 = 7$ with the best system response. The control input $u(t)$ described in (33) has been applied at time $t = 100$ sec as shown in Fig. 7, where the chaos attractor dynamics are suppressed to the stable equilibrium point within a short time. Figure 7(a) shows the phase portrait of motor speed, i_{ds}, and i_{qs} projection, where the red part represents the system dynamics trajectory after applying the control input at $t = 100$ sec. From the motor speed time response in Fig. 7(b), the required response time to stabilize the controlled system is about 4 sec while it is less for motor current components of the motor stator as illustrated in Figs. 7(c) and 7(d).

6. Conclusion

The chaos control in nonlinear systems is an interesting field of research for the last few years. Few studies related to chaos suppression in induction machines drive systems have been published which deals with simple models, fourth-order in maximum. In this paper, eighth-order IFOCIM drive system is derived, IFOCIM system offers different periodicity due to the bifurcation parameter change when the system shows inter chaos in a specific range of the integral gain of the PI speed loop controller. A complex eighth-order IFOCIM drive system is introduced to investigate the chaos oscillation suppression by using fixed-time synergetic control strategy, the fixed-time theory is used to prove that the conventional synergetic control stabilizes the system dynamics within fixed-time boundary not depending on the initial the system vector states, the time upper bound is limited by the FTSC parameters only. The designed control input has been applied to the chaotic IFOCIM drive system at time $t = 100$ sec, the controller forces the system dynamics to leave the chaotic trajectories and converge to the stable equilibrium point within a short time. The system dynamics reach the stable equilibrium point within the fixed-time bound. In future work, the time delay of the controller design can be investigated, and also, the FTSC method can be compared with another control type.

Conflict of Interest

The authors declare that there is no conflict of interests regarding the publication of this paper.

References

Asakura, T., Yoneda, K., Saito, Y. & Shioya, M. [2000] "Chaos detection in velocity control of induction motor and its control by using neural network," *Int. Conf. Signal Proc.* **3**, 1633–1638.

Barambones, O., de Durana, J. & de la Sen, M. [2012] "Robust speed control for a variable speed wind turbine," *Int. J. Innovative Comput. Info. Contr.* **8**, 7627–7640.

Bazanella, A. & Reginatto, R. [2000] "Robustness margins for indirect field-oriented control of induction motors," *IEEE Trans. Automat. Contr.* **45**, 1226–1231.

Borah, M. & Roy, B. [2017] "Dynamics of the fractional-order chaotic PMSG, its stabilisation using predictive

control and circuit validation," *IET Electric Power Appl.* **11**, 707–716.

Bose, B. [2001] *Modern Power Electronics and AC Drives* (Prentice Hall PTR, USA).

Cezayirli, A. & Ciliz, M. [2008] "Indirect adaptive control of non-linear systems using multiple identification models and switching," *Int. J. Contr.* **81**, 1434–1450.

Chang, S. [2020] "Stability, chaos detection, and quenching chaos in the swing equation system," *Math. Probl. Engin.* **2020**, 27–30.

Chen, D., Shi, P. & Ma, X. [2012] "Control and synchronization of chaos in an induction motor system," *Int. J. Innovative Comput. Info. Contr.* **8**, 7237–7248.

Chen, Y., Hagen, C., Olivo, A. & Anastasio, M. [2020] "A partial-dithering strategy for edge-illumination X-ray phase-contrast tomography enabled by a joint reconstruction method," *Phys. Med. Biol.* **65**, 105007.

Chua, K. & Wang, Z. [2011] *Chaos in Electric Drive Systems*: *Analysis*, *Control and Application*, 1st edition (John Wiley & Sons, Singapore).

Fradkov, A. & Evans, R. [2005] "Control of chaos: Methods and applications in engineering," *Ann. Rev. Contr.* **29**, 33–56.

Gao, Y. & Chau, K. T. [2003] "Chaotification of induction motor drives under periodic speed command," *IEEE Power Electronics Specialists Conf.* **31**, 1083–1099.

Gray, R. & Stockham, T. [1993] "Dithered quantizers," *IEEE Trans. Info. Th.* **39**, 805–812.

Harb, A. [2004] "Nonlinear chaos control in a permanent magnet reluctance machine," *Chaos Solit. Fract.* **19**, 1217–1224.

Huang, C., Lin, J., Liao, T., Chen, C. & Yan, J. J. [2011] "Quasi-sliding mode control of chaos in permanent magnet synchronous motor," *Math. Probl. Engin.* **2011**, 1–10.

Huang, S., Linyun, X., Wang, J., Li, P., Wang, Z. & Ma, M. [2020] "Fixed-time synergetic controller for stabilization of hydraulic turbine regulating system," *Renew. Energy* **157**, 1233–1242.

Jain, J. K., Ghosh, S. & Maity, S. [2017] "A numerical bifurcation analysis of indirect vector-controlled induction motor," *IEEE Trans. Contr. Syst. Tech.* **26**, 282–290.

Krishnan, R. & Doran, F. C. [1987] "Study of parameter sensitivity in high-performance inverter-fed induction motor drive systems," *IEEE Trans. Indus. Appl.* **4**, 623–635.

Krishnan, R. & Bharadwaj, A. [1991] "A review of parameter sensitivity and adaptation in indirect vector controlled induction motor drive systems," *IEEE Trans. Power Electr.* **6**, 695–703.

Kumar, M. & Singh, P. [2019] "Chaos control of a four-dimensional fundamental power system using pole placement-based proportional integral sliding mode control," *Int. J. Automat. Contr.* **13**, 679–697.

Landau, I. D. & Lozano, R. [1981] "Unification of discrete time explicit model reference adaptive control designs," *Automatica* **17**, 593–611.

Lu, Y., Li, H. & Li, w. [2009] "Hopf bifurcation and its control in an induction motor system with indirect field oriented control," *2009 4th IEEE Conf. Indus. Electr. Appl. ICIEA* **5**, 3438–3441.

Ni, J. K., Liu, L., Liu, C. X., Hu, X. Y. & Li, S. L. [2017] "Fast fixed-time nonsingular terminal sliding mode control and its application to chaos suppression in power system," *IEEE Trans. Circ. Syst.-II*: *Expr. Briefs* **64**, 151–155.

Ozer, A. B. & Akin, E. [2008] "Chaos control in vector-controlled induction motor drive," *Electr. Power Comp. Syst.* **36**, 733–740.

Rajagopal, K., Vaidyanathan, S., Karthikeyan, A. & Duraisamy, P. [2017] "Dynamic analysis and chaos suppression in a fractional order brushless dc motor," *Electr. Engin.* **99**, 721–733.

Ranjbar, A. & Kholerdi, H. [2016] "Chaotification and fuzzy pi control of three-phase induction machine using synchronization approach," *Chaos Solit. Fract.* **91**, 443–451.

Ren, H. & Liu, H. [2006] "Nonlinear feedback control of chaos in permanent magnet synchronous motor," *IEEE Trans. Circ. Syst. II*: *Express Briefs* **53**, 45–50.

Rongyun, Z., Changfu, G., Peicheng, S., Linfeng, Z. & Changsheng, Z. [2020] "Research on chaos control of permanent magnet synchronous motor based on the synthetical sliding mode control of inverse system decoupling," *J. Vibr. Contr.*, 1077546320936499

Salas, F., Gordillo, F., Aracil, J. & Reginatto, R. [2008] "Codimension-two bifurcations in indirect field oriented control of induction motor drives," *Int. J. Bifurcation and Chaos* **18**, 779–792.

Shang, Z., Yu, Y. & Li, Y. [2020] "Adaptive sliding mode control of chaotic oscillation in power system based on relay characteristic function," *In 2020 IEEE/IAS Industrial and Commercial Power Syst. Asia* (*I&CPS Asia*), pp. 1012–1016.

Sonneveldt, L., Chu, Q. & Mulder, J. [2007] "Nonlinear flight control design using constrained adaptive backstepping," *J. Guid. Contr. Dyn.* **30**, 322–336.

Tahoumi, E., Plestan, F., Ghanes, M. & Barbot, J. [2018] "A controller switching between twisting and linear algorithms for an electropneumatic actuator," *In 2018 European Contr. Conf.* (*ECC*) (IEEE), pp. 2368–2373.

Tarczewski, T. & Grzesiak, L. M. [2016] "Constrained state feedback speed control of PMSM based on model predictive approach," *IEEE Trans. Indust. Electron.* **63**, 3867–3875.

Tu, J. [1996] "Advantages and disadvantages of using artificial neural networks versus logistic regression for predicting medical outcomes," *J. Clin. Epidemiol.* **49**, 1225–1231.

Wang, C., Zhang, H., Fan, W. & Ma, P. [2018] "Adaptive control method for chaotic power systems based on finite-time stability theory and passivity-based control approach," *Chaos Solit. Fract.* **112**, 159–167.

Wang, J., Liu, L., Liu, C. & Liu, J. [2019] "Fixed-time synergetic control for a seven-dimensional chaotic power system model," *Int. J. Bifurcation and Chaos* **29**, 1–14.

Wang, J., Liu, L. & Liu, C. [2020] "Sliding mode control with mismatched disturbance observer for chaotic oscillation in a seven-dimensional power system model," *Int. Trans. Electrical Energy Syst.* **30**, 1–12.

Yao, J., Jiao, Z. & Ma, D. [2015] "A practical nonlinear adaptive control of hydraulic servomechanisms with periodic-like disturbances,' *IEEE/ASME Trans. Mechatr.* **20**, 2752–2760.

Ye, J., Yang, J., Xie, D., Huang, B. & Cai, H. [2019] "Strong robust and optimal chaos control for permanent magnet linear synchronous motor," *IEEE Access* **7**, 57907–57916.

Yu, J., Yu, H., Chen, B., Gao, J. & Qin, Y. [2012] "Direct adaptive neural control of chaos in the permanent magnet synchronous motor," *Nonlin. Dyn.* **70**, 1879–1887.

Yu, J., Chen, B., Yu, H., Lin, C., Ji, Z. & Cheng, X. [2015] "Position tracking control for chaotic permanent magnet synchronous motors via indirect adaptive neural approximation," *Neurocomputing* **156**, 245–251.

Yu, J., Ma, Y., Yu, H. & Lin, C. [2016] "Reduced-order observer-based adaptive fuzzy tracking control for chaotic permanent magnet synchronous motors," *Neurocomputing* **214**, 201–209.

Zhao, L., Huang, J., Chen, J. & Ye, M. [2016] "A parallel speed and rotor time constant identification scheme for indirect field oriented induction motor drives," *IEEE Trans. Power Electr.* **31**, 6494–6503.

Zribi, M., Alrifai, M. T. & Smaoui, N. [2018] "Control of chaos in a single machine infinite bus power system using the discrete sliding mode control technique," *Discr. Dyn. Nature Soc.* **2018**.

Zribi, M., Oteafy, A. & Smaoui, N. [2009] "Controlling chaos in the permanent magnet synchronous motor," *Chaos Solit. Fract.* **41**, 1266–1276.